Biosensors and Bioelectronics 78 (2016) 300–307

Contents lists available at ScienceDirect

Biosensors and Bioelectronics

journal homepage: www.elsevier.com/locate/bios

Reduced graphene oxide-Hemin-Au nanohybrids: Facile one-pot synthesis and enhanced electrocatalytic activity towards the reduction of hydrogen peroxide

Chang-Jie Gu [a], Fen-Ying Kong [b,*], Zhi-Dong Chen [a], Da-He Fan [b], Hai-Lin Fang [b], Wei Wang [b,*]

[a] School of Petrochemical Engineering, Changzhou University, Changzhou 213164, China
[b] School of Chemistry and Chemical Engineering, Yancheng Institute of Technology, Yancheng 224051, China

ARTICLE INFO

Article history:
Received 1 November 2015
Received in revised form
10 November 2015
Accepted 13 November 2015
Available online 14 November 2015

Keywords:
Graphene
Hemin
Au nanoparticles
Hydrogen peroxide
Electrocatalysis

ABSTRACT

A facile and effective strategy is demonstrated for the synthesis of ternary reduced graphene oxide-Hemin-Au (rGO-H-Au) nanohybrids. The nanohybrids were synthesized through a one-pot in situ reduction of GO and $HAuCl_4$ under alkaline conditions using GO, Hemin and $HAuCl_4$ as the starting materials. The synthesis process can be finished within 1 h in a solution phase, without adding any additional surfactant, stabilizing agent and toxic or harsh chemical reducing agents. The resulting nanohybrids were characterized by UV–vis spectroscopy, Raman spectroscopy, transmission electron microscopy (TEM), and so on. Electrochemical measurements showed that the rGO-H-Au nanohybrids exhibited good electrocatalytic activity for the reduction of hydrogen peroxide (H_2O_2). Based on this property, a simple and highly sensitive amperometric biosensor for H_2O_2 had been developed. The linear relationships were obtained from 0.1 μM to 40 μM and the detection limit was estimated to be 30 nM. The simple and sensitive sensing platform showed great promising applications in the pharmaceutical, clinical and industrial detection of H_2O_2.

1. Introduction

In recent years, the synthesis of graphene-based hybrid nanomaterials has sparked enormous research interest due to its potential applications in many fields such as nanoelectronics, nanosensors, batteries (Kuila et al., 2013; Xu et al., 2013). Of particular interest is that graphene's derivative graphene oxide (GO), which is a single-layered two-dimensional sheet, can be considered as versatile nanoscale building blocks to design new and novel graphene-based nanohybrids (Cao et al., 2015; Kong et al., 2012; Oprea et al., 2013; Yang et al., 2014). Up to now, many efforts have been made to hybridize GO with a second or third component to obtain a binary or ternary hybrid nanomaterials, which combines the merits of each component, could provide superior properties over their single components in various applications (Kong et al., 2015a; Li et al., 2015b; Liu et al., 2015; Tu et al., 2010). However, GO is insulating and it should be converted to conducting reduced graphene oxide (rGO) before practical uses. Chemical reduction of GO using reducing agent is probably the most easy and popular method to obtain rGO. In the process of reduction, reducing agents such as hydrogen sulfide, hydrazine, sodium borohydride and hydroquinone are usually employed. Unfortunately, they are very hazardous and they also can introduce additional functional groups during reduction, increasing sheet resistance by scattering electrons (Kong et al., 2015b; Lei et al., 2014; Zhao et al., 2015). Moreover, most preparation processes are complicated, multi-steps and time-consuming. It is therefore great promising to develop a simple, rapid and cost-effective route for the synthesis of complex graphene-based hybrids.

As the active center of hemin-protein family, hemin (H) has been widely used, because it is cheap, stable and able to catalyze the reduction reactions of H_2O_2 (Cao et al., 2012; Chen et al., 2011). In particular, hemin can be well used as electron media based on the reversible Fe (III)/Fe (II) redox couple, and exhibits good electrocatalysis to many small molecules related to life process (Kong et al., 2015a). However, direct application of hemin as a catalyst leads to passivation because hemin is sparingly soluble in water and produces molecular aggregation of the inactive dimers (Zhang et al., 2014). One solution to this problem would be to load hemin on some supporting materials which can provide suitable microenvironments to prevent the dimerization of hemin. Among

* Corresponding authors.
E-mail addresses: kongfy@ycit.edu.cn (F.-Y. Kong), kongfy@ycit.edu.cn (W. Wang).

http://dx.doi.org/10.1016/j.bios.2015.11.035
0956-5663/

the efforts, the technique of immobilizing hemin on graphene through aromatic π–π interaction was found to be very promising due to its improved electron transfer, enhanced electrostatic interaction, excellent electrocatalytic response, peroxidase-like activity and easy preparation (Wei et al., 2012).

Au nanoparticles (Au NPs) have a large specific surface area, good biocompatibility and excellent conductivity. Au NPs can enhance the electron transfer between redox centers in biomolecules and electrode surfaces and can act as catalysts to increase the rate of electrochemical reactions (Kong et al., 2011). Especially, Au NPs exhibit excellent electrocatalytic activity towards the reduction of H_2O_2 (Jirkovský et al., 2010; Saha et al., 2012; Zeis et al., 2008). Nevertheless, Au NPs usually tend to aggregate owing to its high surface energy (Yin et al., 2012). Recent studies demonstrate that graphene has significant potential as a supporting material for immobilizing and stabilizing of metal particles, for the development of new electrocatalysis systems (Jing et al., 2015; Li et al., 2015a; Maji et al., 2015).

In this work, we have developed a one-pot strategy for synthesizing ternary reduced graphene oxide-Hemin-Au (rGO-H-Au) nanohybrids by simply heating GO, hemin and metal precursors under alkaline conditions, without adding any additional surfactant, stabilizing agent and reducing agents. In this easy method, GO nanosheets are not only used as carrier for hemin but also used as reducing agents, stabilizing agent and carrier for in situ growing of Au NPs. In turn, the formed Au NPs serve as the catalyst to accelerate the reduction of GO. This easy one-pot procedure provides a new pathway for simply and rapid preparing of graphene-based multicomponent nanomaterials. What's more, the synthesized ternary rGO-H-Au nanohybrids exhibit good biocompatibility, fast redox property and remarkable electrocatalysis towards the reduction of H_2O_2. Based on the nanohybrids, a simple and sensitive amperometric biosensor for H_2O_2 has been developed.

2. Experimental

2.1. Reagents

Graphite powder and Tetrachloroauric acid ($HAuCl_4$) were purchased from Aladdin Reagent Co. Ltd. (Shanghai, China). H_2O_2 (30 wt% in H_2O), $NaNO_3$ were obtained from Beijing Chemical Reagent Company. Hemin (ferriprotoporphyrin IX chloride, 98 wt%) was obtained from Sigma. Unless otherwise stated, the chemicals in this work were of analytical grade and used as received without further purification. H_2O_2 solutions were freshly prepared before used. Phosphate buffer solutions (PBS) were prepared by mixing stock solutions of NaH_2PO_4 and $NaHPO_4$. All aqueous solutions were prepared with ultrapure water from a Milli-Q Plus system (Millipore).

2.2. Instruments

UV–vis absorption spectra were recorded on a UV-2150 spectrophotometer (Shimadzu, Japan). Fourier transform infrared spectroscopy (FT-IR) experiments were performed on a Tensor 27 FT-IR spectrometer (Bruker, Germany). The transmission electron microscopic (TEM) images were acquired with a JEOL mode 2000 instrument operated at 200 kV (JEOL Ltd., Japan). Resonance Raman spectra were measured on a LabRAM HR 800 Raman spectrophotometer (Jobin Yvon, France). X-ray diffraction (XRD) data were recorded in the range of 2θ by step scanning on the Bruker D8 Advance (superspeed) diffractometer (Bruker-AEX, Germany) with Cu Kα radiation (k=0.15406 nm) operated at 40 kV and 100 mA. Electrochemical measurements were performed on a CHI 840 C electrochemical workstation (Shanghai Chenhua Instruments, China) with a standard three-electrodes system composed of platinum wire as an auxiliary electrode, Ag/AgCl electrode as a reference electrode, and the modified glassy carbon electrode (GCE, 3 mm in diameter) as a working electrode.

2.3. Preparation of rGO-H-Au nanohybrids

GO was synthesized from natural graphite powder by a modified Hummers method reported in our previous work (Kong et al., 2015b). The freshly prepared GO was dispersed in ultrapure water by ultrasonication to obtain a yellow-brown aqueous GO solution. Then, 10.0 mL of GO solution (1 mg mL^{-1}) were mixed with 10.0 mL 1 mg mL^{-1} hemin dissolved in ethanol, followed by the addition of 0.2 mL 0.02425 mol L^{-1} $HAuCl_4$ solution. Subsequently, 0.5 mol L^{-1} NaOH solution was added dropwise into the above mixture until pH was 10.0. After vigorous shaking and sonication for 0.5 h at room temperature, the flask containing the mixture was placed in an oil bath (100 °C) with refluxing for 1 h. Finally, the stable black dispersion was obtained and further centrifuged at 12,000 rpm for 20 min to remove the supernatant. The obtained production (rGO-H-Au nanohybrids) were steadily dispersed in ultrapure water and used for further experiments.

2.4. Fabrication of rGO-H-Au nanohybrids modified electrode

Prior to experiment, GCE was carefully polished with 1.0, 0.3 and 0.05 μm alumina powder separately until a mirror like surface was achieved, followed by being sonicated in alcohol and water successively and dried in nitrogen. Subsequently, 5 μL of rGO-H-Au suspension was coated onto the surface of GCE and dried in air. Similarly, rGO/GCE and rGO-H/GCE were also prepared for comparison.

3. Results and discussion

3.1. Principles

In a simple and facile approach, stable and water dispersible ternary rGO-H-Au nanohybrids were prepared by heating the GO, hemin and $HAuCl_4$ under alkaline conditions. And the obtained rGO-H-Au nanohybrids were used to construct a sensor for the determination of H_2O_2. Fig. 1 is schematic of the preparation of rGO-H-Au nanohybrids (A) and the principle of determination H_2O_2 (B). In this process, hemin molecules were firstly loaded on the surface of GO sheets through π–π interaction. Here, GO used as supporting materials to prevent the dimerization of hemin. Meanwhile, the adsorbed hemin molecules enable the followed formed rGO from restacking. In addition, the conjugated GO-H can act as the initial precursor for immobilizing and stabilizing of Au NPs. As it is well known that both GO and hemin contain plentiful and reactive groups, such as hydroxyl, carboxyl, epoxide groups in GO and carboxyl, alkylene groups in hemin (Kuila et al., 2013). These functional groups of GO-H provide anchor sites for the nucleation and growth of metal NPs. In the process of heating and refluxing, Au NPs are in situ generated on the surface of GO-H and GO was reduced into rGO simultaneously under alkaline conditions. It is noteworthy that not only alkaline conditions with heating but also GO and ethanol help to reduce $HAuCl_4$ to Au NPs. In turn, the formed Au NPs can serve as the catalyst to accelerate the reduction of GO. As a result, the whole synthesis process can be finished in 1.5 h and the obtained rGO-H-Au nanohybrids are highly stable and well dispersible in water. In our case, none of additional surfactant, stabilizing agent and reducing agents is employed. It provides a new pathway for simply and effectively preparing of graphene-based multicomponent nanomaterials. The

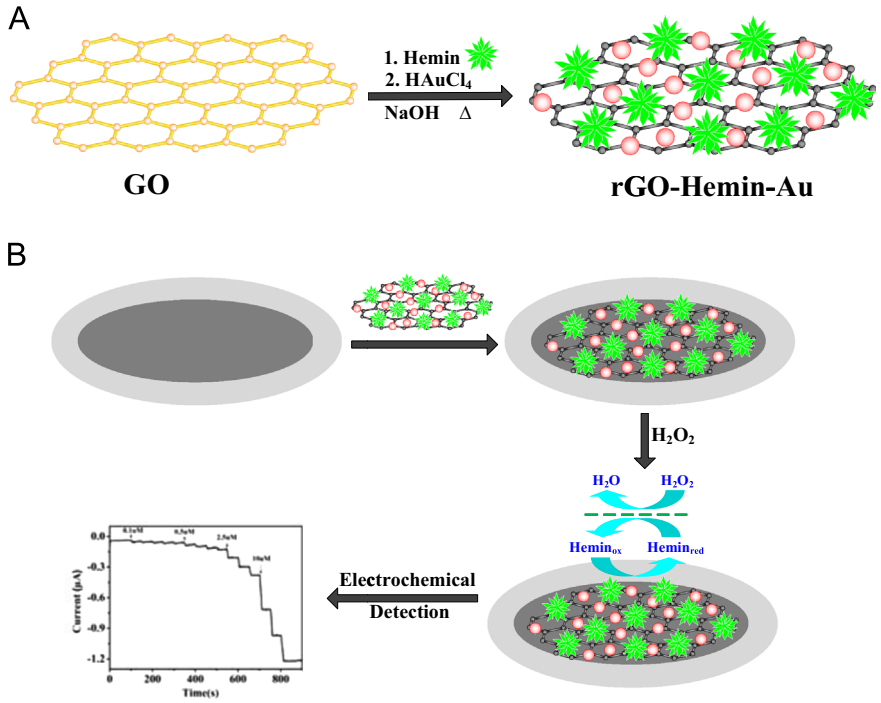

Fig. 1. Schematic of the preparation of rGO-H-Au nanohybrids (A) and the principle of determination H_2O_2 (B).

as-obtained nanohybrids are subsequently coated on the GCE surface for determination of H_2O_2. H_2O_2 is an important analyte in biochemical, industrial and environmental systems. Therefore, the determination of H_2O_2 is very important. It is reported that there exist reactions between hemin Fe (II) and H_2O_2. In the reaction, H_2O_2 was reduced to H_2O while Fe (III) was first reduced to Fe (II) species and then back to the initial state (Tu et al., 2010).

3.2. Characterization of the rGO-H-Au nanohybrids

The evidence demonstrating the successful synthesis of rGO-H-Au nanohybrids are firstly supplied by UV–vis absorption spectra (Fig. 2A). As shown in curve a, the GO displays a strong absorption band centered at approximately 235 nm and a shoulder absorption band at 300 nm which is attributed to π–π^* transitions of the aromatic C=C band and n–π^* transitions of the C=O band, respectively (Vernekar and Mugesh, 2012). The spectra of the hemin solution contains a strong absorption band at 387 nm corresponding to the Soret band of hemin, as well as a group of weak absorption bands between 500 and 700 nm ascribed to Q-bands of hemin (curve b). After heating GO-H conjugation under alkaline conditions, the absorption band of GO around 235 nm red shifts to about 260 nm and the absorption band at 300 nm disappeared, which is consistent with the characters of rGO. At the same time, the maximum absorption band of hemin red shifts 33 nm, indicating the existence of π–π interaction between rGO and hemin molecules (Bi et al., 2014; Hu et al., 2014; Song et al., 2013). As for the rGO-H-Au nanohybrids (curve d), a new absorption band appears at approximately 540 nm compared with curve c, which correspond to the surface plasmon absorption of Au nanoparticles. These phenomena indicate that the hemin molecules combine with rGO through noncovalent π–π interactions and Au nanoparticles generate on the surface of rGO-H conjugation and form rGO-H-Au nanohybrids.

FT-IR spectra can provide some useful information on the structure of rGO-H-Au nanohybrids. Fig. 2B shows the comparative

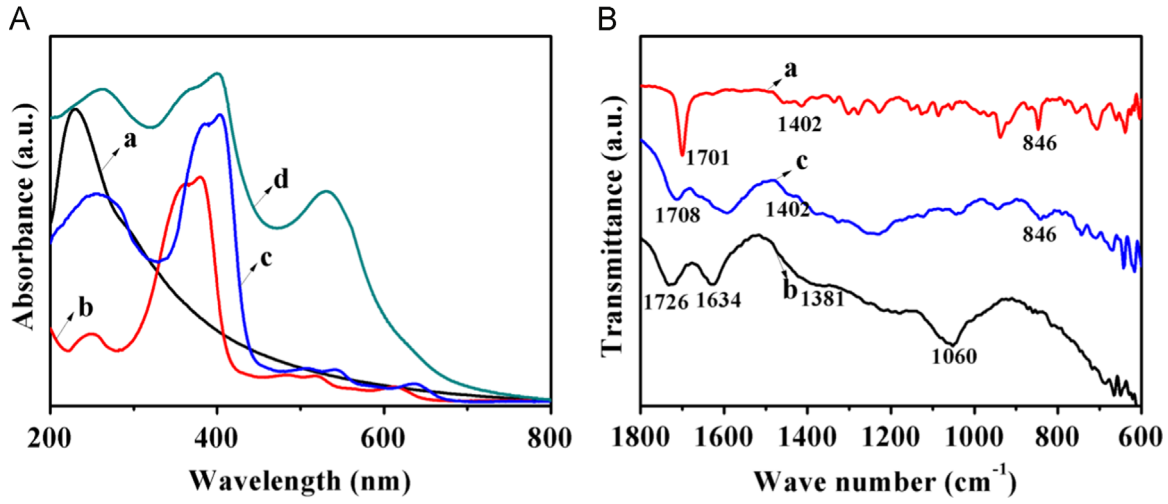

Fig. 2. (A) UV–vis absorption spectra of GO (a), Hemin (b), rGO-H (c) and rGO-H-Au nanohybrids (d). (B) FT-IR spectra of Hemin (a), GO (b) and rGO-H-Au nanohybrids (c).

FT-IR spectra of hemin, GO and rGO-H-Au nanohybrids. As shown in curve a, the FT-IR spectra of hemin shows an absorption band assigned to the C=O stretch mode of carboxylic group at 1701 cm^{-1}, an absorption band attributed to the B3u vibration of porphyrin at 1402 cm^{-1} and =C–H deformation vibration of olefin at 846 cm^{-1}, which are consistent with the reported literatures (Tu et al., 2009; Xu et al., 2009; Zhang et al., 2013). The spectra of GO (curve b) reveals an absorption band at 1726 cm^{-1} due to C=O stretching of GO. Stretching vibrations at 1634 cm^{-1}, 1381 cm^{-1} and 1060 cm^{-1} are attributed to the C=C, C–H and C–O units in GO, respectively (Li et al., 2015a). After formation of rGO-H-Au nanohybrids (curve c), the characteristic absorption for vibrations from C=O has disappeared in comparison with GO. And a dramatic decrease in the absorption of C–O and O–H groups is observed, which indicate that the most of oxygen containing groups has been effectively removed by the hydrothermal reduction. In contrast to pure hemin, the absorption band assigned to the C=O stretching vibration shifts from 1701 cm^{-1} to 1708 cm^{-1}, which attributed to the π–π aromatic interactions between the hemin and rGO (Wei et al., 2012). These results confirm that GO has been effectively reduced to rGO and the hemin has been succefully loaded on the surface of rGO by the hydrothermal method.

Raman spectroscopy was also used to demonstrate the formation of rGO-H-Au nanohybrids. Fig. 3A shows the Raman spectra of the GO, hemin and rGO-H-Au nanohybrids. It can be clearly seen that there are two prominent peaks in GO around 1594 cm^{-1} and 1351 cm^{-1} (curve a), which correspond to the sp^2-bonded carbon atoms in a hexagonal lattice (G band) and the vibration of sp^3-bond carbon atoms of defects and disorder (D band), respectively (Li et al., 2015a). As shown in curve b, the Raman spectra of hemin displays three major bands located at 1632 cm^{-1}, 1574 cm^{-1}, and 1368 cm^{-1}. The former two peaks are related to the asymmetric C–C stretching and the latter is attributed to the symmetric pyrrole-half-ring stretching of the protoporphyrin (IX) ring system, respectively (Cao et al., 2012; Huang et al., 2014; Xu et al., 2009). Compared with pure GO and hemin, a slight increased D/G intensity ratio is observed and three characteristic peaks of hemin remained in the spectra of rGO-H-Au nanohybrids (curve c), confirming that GO is converted into rGO and hemin molecules are attached onto rGO successfully in our experiments (Li et al., 2013; Wei et al., 2013).

XRD analysis are further investigated for the as-synthesized GO (curve a), hemin (curve b) and rGO-H-Au (curve c) nanohybrids as shown in Fig. 3B. A broad peak around 24.2° can be observed for all of them, which corresponds to the characteristic diffraction peak C(002) (Zhao et al., 2015). XRD patterns of hemin (curve b) show two sharp peaks at 30.32° and 35.58°, which can be assigned to cubic crystalline magnetite Fe_3O_4 phase (JCPDS no. 01-088-0315) (Wang et al., 2010). The Fe_3O_4 phase may be formed through the oxidation of Fe in hemin by the trace dioxygen in the atmosphere. In addition, there are five strong diffraction peaks in rGO-hemin-Au nanohybrids (curve c) which can be indexed to the (111), (200), (220), (311) and (222) planes of the Au NPs (JCPDS no. 01-1172) (Lv and Weng, 2013; Zhang et al., 2011).

The morphology and microstructure of the obtained nanohybrids are characterized by Transmission electron microscopy (TEM) and the results are shown in Fig. 4. As can be seen, Fig. 4A shows a layer of GO with a wrinkled flake-like structure, which benefits from the high surface of GO (Zhang et al., 2011). As for rGO-H conjugation, a relatively flat surface without wrinkle appears (Fig. 4B), which can be interpreted as that the aggregated hemin molecules attach on the surface of rGO uniformly through π–π interaction (Jiang et al., 2012). From the TEM images of Fig. 4C and D, it clearly reveals that the approximate spherical Au NPs with an average diameter of about 6 nm evenly disperse on the surface of rGO-H conjugation.

3.3. Electrochemical behaviors of the rGO-H-Au nanohybrids modified electrode

Cyclic voltammograms (CVs) are applied to study the electrochemistry properties of different electrodes. Fig. 5 displays CV curves of bare, GO, rGO-H and rGO-H-Au nanohybrids modified GCE in the absence (A) and presence (B) of H_2O_2 in the potential range of −0.6 to 0.4 V in 0.1 M PBS (pH 7.0) saturated with N_2. As can be seen from Fig. 5A, the CV responses of bare GCE and GO/GCE in PBS don't show any observable peak (curve a and b). When rGO-H conjugation is coated onto the electrode surface, a couple of obvious redox peaks is observed (curve c). The redox peaks should be attributed to hemin, which is the characteristic of a single electron transfer process of iron at the core of hemin for the $hemin_{ox}/hemin_{red}$ pair. As expected, rGO-H-Au/GCE exhibits higher redox peak currents of hemin (curve d), revealing that the introduction of Au NPs can greatly facilitate the electron transfer between hemin and the electrode. The inset of Fig. 5A proves the existence of Au NPs again by comparing rGO-H/GCE with rGO-H-Au/GCE in a wider potential range, since that the CV response of the latter emerge a more oxidation peak at about 0.6 V corresponding to the oxidation of Au NPs.

Moreover, these modified electrodes are used to investigate the

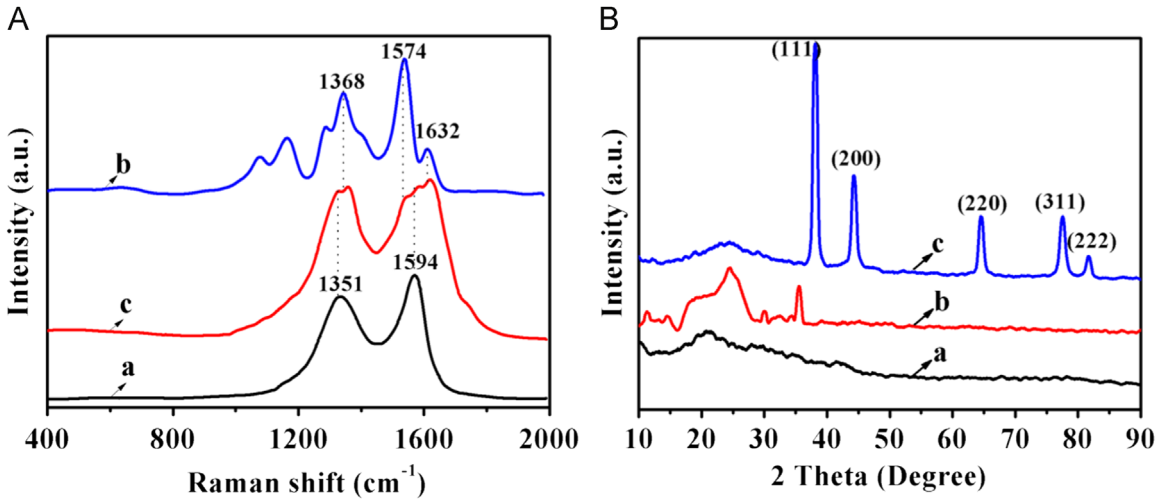

Fig. 3. (A) Raman spectra of GO (a), hemin (b) and rGO-H-Au nanohybrids (c). (B) XRD patterns of GO (a), hemin (b) and rGO-H-Au nanohybrids (c).

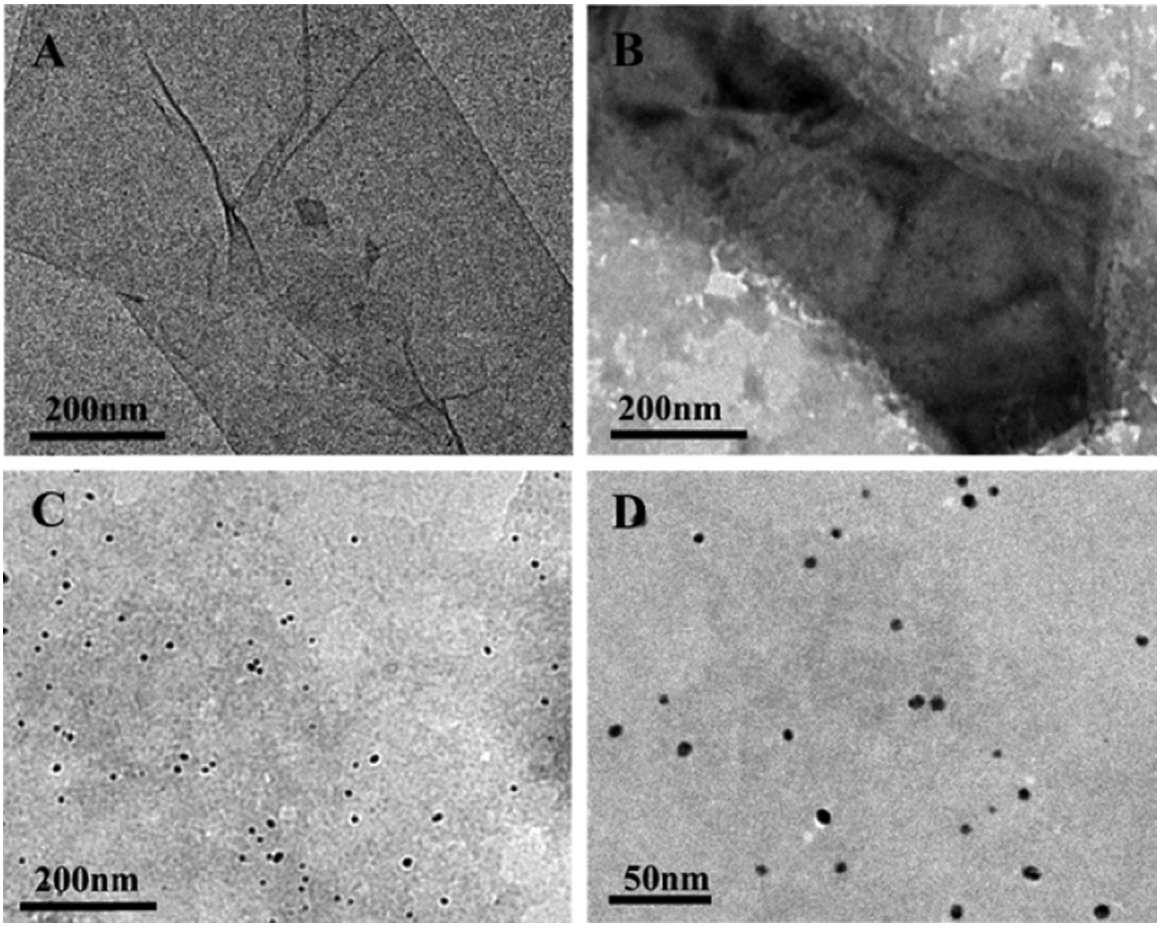

Fig. 4. TEM images of GO (A), rGO-H (B) and rGO-H-Au nanohybrids (C and D).

electrocatalytic activity toward the reduction of H_2O_2. As shown in Fig. 5B, no obvious reduction peak could be observed at bare GCE or GO/GCE when 10 μM H_2O_2 is added into N_2-saturated PBS (curve a and b). When the electrode is modified with rGO-H conjugation (curve c), a new weak reduction peak centered at −0.18 V appears. It corresponds to the response of H_2O_2, in which H_2O_2 is reduced to H_2O while Fe (III) is first reduced to Fe (II) species and then back to the initial state (Cao et al., 2012; Lei et al., 2014; Zhang et al., 2014). Compared to rGO-H/GCE, the CV response of H_2O_2 at rGO-H-Au/GCE improves greatly (curve d). This excellent performance is attributed to the high electron transfer rate of rGO and the synergistic interaction of three components.

The electrocatalytic behavior of rGO-H-Au/GCE toward different concentrations of H_2O_2 is also studied by CVs. As seen from Fig. 6A, rGO-H-Au/GCE displays nice responses to different concentrations of H_2O_2 in N_2-saturated PBS (pH 7.0), which indicates that rGO-H-Au nanohybrids exhibit a high electrocatalytic activity

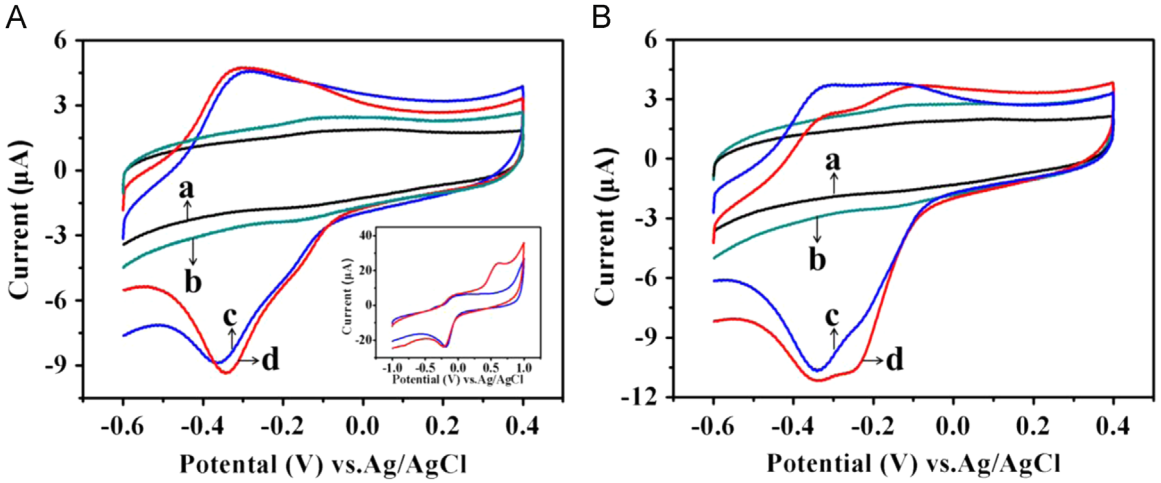

Fig. 5. (A) CV curves of bare GCE (a), GO/GCE (b), rGO-H/GCE (c), rGO-H-Au/GCE (d) in N_2-saturated 0.1 M PBS (pH 7.0). Inset: CV curves of rGO-H/GCE (blue) and rGO-H-Au/GCE (red). (B) CV curves of bare GCE (a), GO/GCE (b), rGO-H/GCE (c), rGO-H-Au/GCE (d) in the presence of 10 μM H_2O_2 in N_2-saturated 0.1 M PBS (pH 7.0). Scan rate: 100 mV s^{-1}. (For interpretation of the references to color in this figure legend, the reader is referred to the web version of this article.)

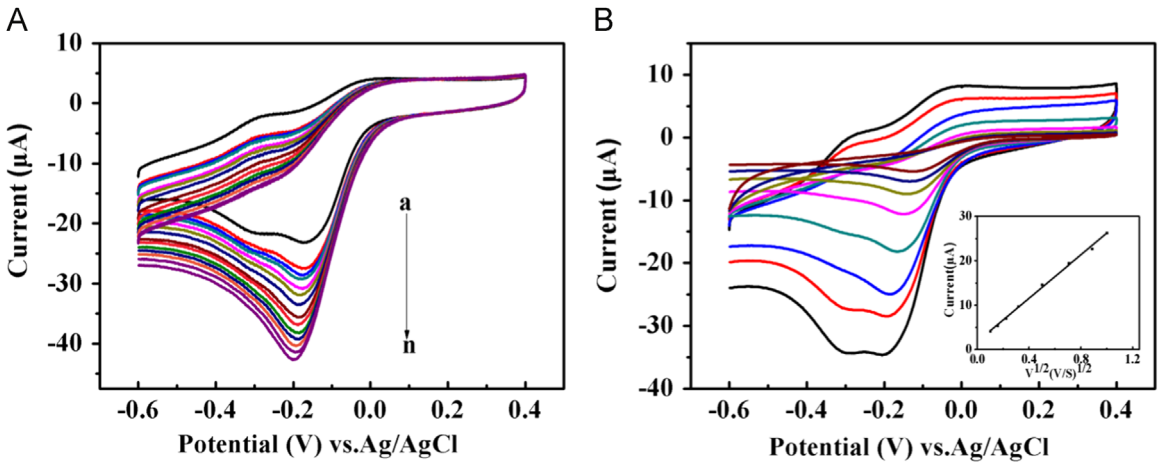

Fig. 6. (A) CV curves of rGO-H-Au/GCE (a) in 0.1 M PBS (pH 7.0) with a successive addition of 10 μM H_2O_2 (b→n) at scan rates of 100 mV s^{-1}. (B) CV curves of rGO-H-Au/GCE in 0.1 M PBS (pH 7.0) containing 20 μM H_2O_2 at different scan rates of 10, 25, 50, 100, 250, 500, 750, 1000 mV s^{-1} (correspoding to a→h). Inset shows peak current as a function of scan rate at the electrode subject to 20 μM H_2O_2 in 0.1 M PBS (pH 7.0).

towards the reduction of H_2O_2. Apparently, the reduction peak currents increase gradually with increasing concentrations of H_2O_2 (0, 10, 20, 30, 40, 50, 60, 70, 80, 90, 100, 110, 120 and 130 μM corresponding to curves a to n). Furthermore, the CVs of rGO-H-Au/GCE at various scan rates in N_2-saturated 0.1 M PBS (pH 7.0) containing 20 μM H_2O_2 are investigated in Fig. 6B. The reduction peak currents vary linearly with the function of scan rates in a range of 10–1000 mV s^{-1}, as shown in the inset of Fig. 6B. This suggests that the electron transfer process for the rGO-H-Au/GCE belongs to a surface-confined mechanism in the potential scope mentioned above.

3.4. Amperometric sensing of H_2O_2

On the basis of above results, a biosensor at rGO-H-Au/GCE for the quantitative determination of H_2O_2 is developed. The performance of rGO-H-Au/GCE towards the determination of H_2O_2 is evaluated by amperometry, which is one of the most widely employed techniques for biosensor. Fig. 7A shows amperometric responses of rGO-H-Au/GCE at −0.18 V upon the addition of an aliquot of H_2O_2 to the stirring buffer solution. The reductive current rises steeply to reach a stable value within 50 s, which indicates a fast process. As shown in Fig. 7B, the current responses are proportional to the H_2O_2 concentration in a range from 0.1 μM to 40 μM, and the regession equation is I (μA)=0.05311+0.03007*c* (μM) with a correlation coefficient of 0.9956. The detection limit is estimated to be 30 nM (*S*/*N*=3). Compared with previously reported hemin related sensors for the determination of H_2O_2 (Table 1), the rGO-H-Au/GCE shows a wider linear range and a lower detection limit. The excellent performance benefits from the synergetic effects of rGO (high conductivity and large surface are), of the hemin (excellent catalysis and intrinsic peroxidase-like activity) and of the Au NPs (good biocompatibility and high-speed electron transfer).

3.5. Selectivity, reproducibility and stability of the biosensor

In order to test the applicability of this H_2O_2 sensor with real samples, some possibly coexisting interferents, such as uric acid (UA), ascorbic acid (AA), dopamine (DA) and cysteine (Cys) are subsequently investigated. Fig. 8 shows the amperometric responses for the biosensor of subsequent injection of H_2O_2, UA, AA, DA, Cys and H_2O_2 at −0.18 V. It is evident from the trace of the response current that the influence of the tested interfering species on the response of the H_2O_2 is insignificant. This phenomenon indicates that the novel biosensor is highly selective for H_2O_2. In addition, the reproducibility of the electrode is investigated at a H_2O_2 concentration of 10 μM, the relative standard deviation (RSD) was 3.5% for eight consecutive measurements. It confirms that the fabrication method is highly reproducible. Moreover, the

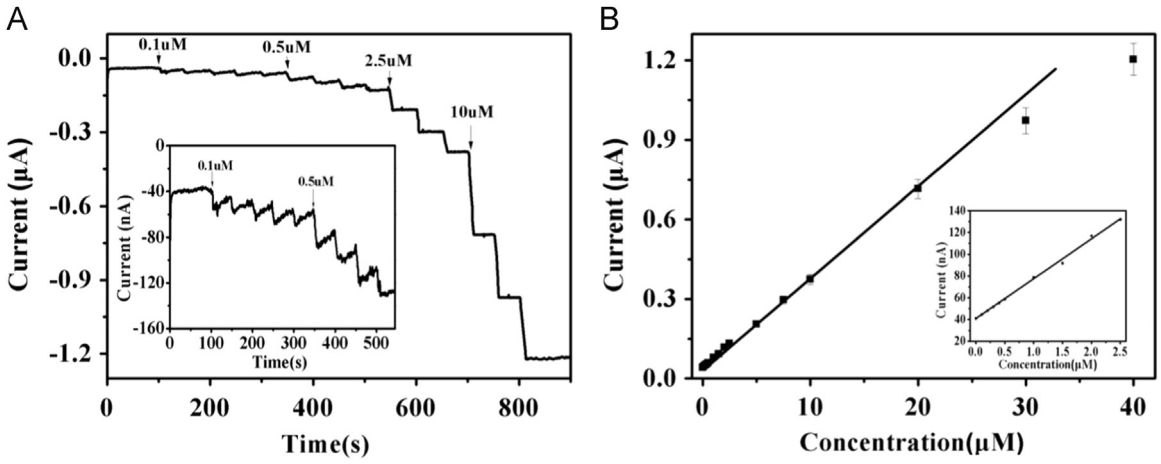

Fig. 7. (A) Typical current–time response curve of the biosensor upon successive additions of H_2O_2 at an applied potential of −0.18 V and inset shows amplified response curve. (B) Linear calibration of current-concentration and inset shows linear calibration at low concentration.

Table 1
Comparison of performances of various electrodes for H_2O_2 detection.

Modified electrode	Linear range/μM	Detection limit/μM	Applied potential/V versus Ag/AgCl	References
GN-Hemin-SWCNT/GCE	0.2–400	0.05	−0.2	Kong et al. (2015a)
Hemin-graphene-PEDOT/GCE	0.5–70	0.08	−0.2	Lei et al. (2014)
CCG-hemin/GCE	96–1440	–	−0.09	Chen et al. (2011)
Hemin-OMC-Nafion/GCE	2–250	0.3	−0.4	Cao et al. (2012)
Nafion/LDH-hemin/PGE	1–240	0.3	−0.4	Zhang et al. (2014)
Hemin-GNs-AuNPs/GCE	0.3–1800	0.11	−0.2	Song et al. (2013)
PPY-He-RGO/GCE	0.5–80	0.13	−0.15	Huang et al. (2014)
Hemin-GNs/GCE	0.5–400	0.2	−0.2	Guo et al. (2011)
RGO-H-Au/GCE	0.1–40	0.03	−0.18	This work

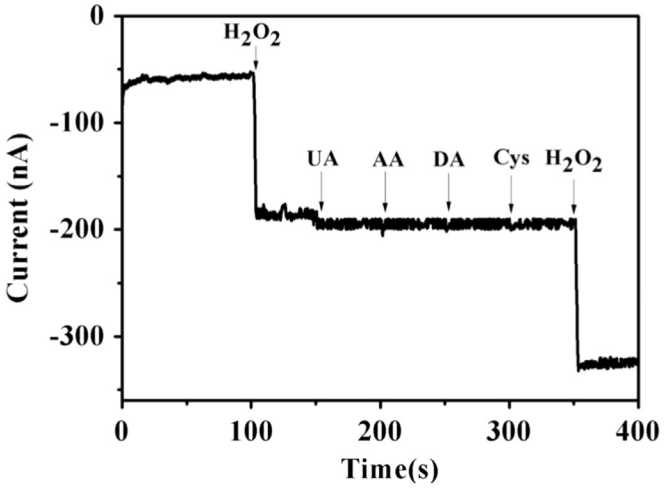

Fig. 8. Amperometric responses of rGO-H-Au/GCE in N_2-saturated 0.1 M PBS (pH 7.0) at −0.18 V for the sequential addition of 10 μM H_2O_2, 100 μM UA, 100 μM AA, 100 μM DA, 100 μM Cys and 10 μM H_2O_2.

stability of modified electrode has also been studied. After modifying the electrode, the rGO-H-Au/GCE is stored in the refrigerator for 8 h, 1 day, 2 day, 4 day, 8 day, 16 day, 30 day, respectively. There is no obvious change after storage below 8 days. It retained 91.6% and 80.6% of its initial amperometric response after 16 days and 30 days. These results indicate that the modified electrodes have satisfying stability.

4. Conclusions

In conclusion, we have demonstrated in this paper that ternary rGO-H-Au nanohybrids can be easily prepared by simple mixing of GO, hemin with $HAuCl_4$ and heating under alkaline conditions without using any additional surfactant, stabilizing agent and reducing agents. The procedure is highly efficient and time-saving, as the whole synthesis process can be finished in 1.5 h. The approach provides a potential for preparing other multi-component hybrids based on different metal precursors. Significantly, the rGO-H-Au nanohybrids combine the main excellent properties of the three components, maintaining the peroxidase-like activity of hemin, and displaying a high-speed electron transfer ascribed to the presence of rGO sheets and Au NPs. In addition, the sufficient accessible specific area of graphene also provides a superb opportunity for a high loading of hemin and Au NPs within the composite matrix. Based on these good properties, the rGO-H-Au nanohybrids exhibited remarkable electrocatalysis towards the reduction of H_2O_2 with satisfying stability, selectivity, and simplicity. We think that the simple preparation process and the excellent performance make rGO-H-Au nanohybrids a promising hybrid nanomaterials for many other applications, such as artificial enzyme mimetics, electrocatalysis, luminescence, and electronics, etc.

Acknowledgments

This work was supported by the National Natural Science Foundation of China (21575123 and 21305122), the Natural Science Foundation of Jiangsu Province (BK20131218), the Opening Foundation of the State Key Laboratory of Analytical Chemistry for Life Science of Nanjing University (SKLACLS1312), and the Industry-University-Research Cooperative Innovation Foundation of Jiangsu Province (BY2015057-17, BY2014108-08, BY2014108-19).

Reference

Bi, S., Zhao, T.T., Jia, X.Q., He, P., 2014. Biosens. Bioelectron. 57, 110–116.
Cao, H.M., Sun, X.M., Zhang, Y., Hu, C.Y., Jia, N.Q., 2012. Anal. Methods 4, 2412–2416.
Cao, X., Gao, J., Ye, Y.P., Ding, S., Ye, Y., Sun, H., 2015. Electroanal. 27, 1–6.
Chen, J., Zhao, L., Bai, H., Shi, G., 2011. J. Electroanal. Chem. 657, 34–38.
Guo, Y., Li, J., Dong, S., 2011. Sens. Actuators B 160, 295–300.
Hu, C., Xi, Q., Ge, J., Luo, F.Y., Tang, L.J., Jiang, J.H., Yu, R.Q., 2014. RSC Adv. 4, 64252–64257.
Huang, W., Hao, Q., Lei, W., Wu, L., Xia, X., 2014. Mater. Res. Express 1, 045601–045617.
Jiang, R., Tran, D.T., McClure, J., Chu, D., 2012. Electrochem. Commun. 19, 73–76.
Jing, P., Yi, H., Xue, S., Chai, Y., Yuan, R., Xu, W., 2015. Anal. Chim. Acta 853, 234–241.
Jirkovský, J.S., Halasa, M., Schiffrin, D.J., 2010. Phys. Chem. Chem. Phys. 12, 8042–8052.
Kong, F.Y., Li, X.R., Zhao, W.W., Xu, J.J., Chen, H.Y., 2012. Electrochem. Commun. 14, 59–62.
Kong, F.Y., Xu, Z., Xu, M.T., Xu, J.J., Chen, H.Y., 2011. Electrochim. Acta 56, 9386–9390.
Kong, F.Y., Li, W.W., Wang, J.Y., Fang, H.L., Fan, D.H., Wang, W., 2015a. Anal. Chim. Acta 884, 37–43.
Kong, F.Y., Li, W.W., Wang, J.Y., Wang, W., 2015b. Biosens. Bioelectron. 69, 206–212.
Kuila, T., Mishra, A.K., Khanra, P., Kim, N.H., Lee, J.H., 2013. Nanoscale 5, 52–71.
Lei, W., Wu, L., Huang, W., Hao, Q., Zhang, Y., Xia, X., 2014. J. Mater. Chem. B 2, 4324–4330.
Li, W.W., Kong, F.Y., Wang, J.Y., Chen, Z.D., Fang, H.L., Wang, W., 2015a. Electrochim. Acta 157, 183–190.
Li, Y., Deng, J., Fang, L., Yu, K., Huang, H., Jiang, L., Liang, W., Zheng, J., 2015b. Biosens. Bioelectron. 63, 1–6.
Li, Y.J., Huang, X.Q., Li, Y.J., Xu, Y., Wang, Y., Zhu, E.B., Duan, X.F., Huang, Y., 2013. Sci. Rep. 3, 1787–1793.
Liu, J., Xin, X., Zhou, H., Zhang, S., 2015. Chem. Eur. J. 21, 1908–1914.
Lv, X.C., Weng, J., 2013. Sci. Rep. 3, 3285–3294.
Maji, S.K., Mandal, A.K., Nguyen, K.T., Borah, P., Zhao, Y.L., 2015. ACS Appl. Mater. Interfaces 7, 9807–9816.
Oprea, R., Peteu, S.F., Subramanian, P., Qi, W., Pichonat, E., Happy, H., Bayachou, M., Boukherroub, R., Szunerits, S., 2013. Analyst 138, 4345–4352.
Saha, K., Agasti, S.S., Kim, C., Li, X.N., Rotello, V.M., 2012. Chem. Rev. 112, 2739–2779.
Song, H., Ni, Y., Kokot, S., 2013. Anal. Chim. Acta 788, 24–31.
Tu, W.W., Lei, J.P., Ding, L., Ju, H.X., 2009. Chem. Commun. 28, 4227–4229.
Tu, W.W, Lei, J.P., Zhang, S., Ju, H.X., 2010. Chem. Eur. J. 16, 10771–10777.
Vernekar, A.A., Mugesh, G., 2012. Chem. Eur. J. 18, 15122–15132.
Wang, Q., Zhou, Z., Chen, D., Lin, J., Ke, F., Xu, G., Sun, S., 2010. Sci. China Chem. 53, 2057–2062.
Wei, J., Qiu, J., Li, L., Ren, L., Zhang, X., Chaudhuri, J., Wang, S., 2012. Nanotechnology 23, 335707–335713.
Wei, W., Zhang, D.M., Yin, L.H., Pu, Y.P., Liu, S.Q., 2013. Spectrochim. Acta A 106, 163–169.
Xu, M.S., Liang, T., Shi, M.M., Chen, H.Z., 2013. Chem. Rev. 113, 3766–3798.

Xu, Y., Liu, Z., Zhang, X., Wang, Y., Tian, J., Huang, Y., Ma, Y., Zhang, X., Chen, Y., 2009. Adv. Mater. 21, 1275–1279.
Yang, Z.T., Qian, J., Yang, X.W., Jiang, D., Du, X.J., Wang, K., Mao, H., Wang, K., 2014. Biosens. Bioelectron. 65C, 39–46.
Yin, H., Tang, H., Wang, D., Gao, Y., Tang, Z., 2012. ACS Nano 6, 8288–8297.
Zeis, R., Lei, T., Sieradzki, K., Snyder, J., Erlebacher, J., 2008. J. Catal. 253, 132–138.
Zhang, F.T., Long, X., Zhang, D.W., Sun, Y.L., Zhou, Y.L., Ma, Y.R., Qi, L.M., Zhang, X.X., 2014. Sens. Actuators B 192, 150–156.
Zhang, J., Liu, X., Wang, L., Yang, T., Guo, X., Wu, S., Zhang, S., Wang, S., 2011. Carbon 49, 3538–3543.
Zhang, Y.F., Xu, C.L., Li, B.X., 2013. RSC Adv. 3, 6044–6050.
Zhao, Y., Zhang, L., Wei, W., Li, Y., Liu, A., Zhang, Y., Liu, S., 2015. RSC Adv. 5, 82879–82886.